CHAPTER VI
EVENT SIMULATION AND THEORY II: POMERON

This chapter paves path for data analysis where one deals with two questions: (1) how do we correct the raw data? and (2) how do we interprete the results in theoretical context? In today's high energy experiments, Monte Carlo simulation of both the physics process and experiment provides a most effective tool. Simulation of the ZEUS experiment is mainly done by MOZART and ZGANA programs(see Chapter III, Section 3.2.6). Simulation of the physics process is technically simpler. Final states are generated according to theoretical differential cross section and hadronization probabilty, with aid of random number generators.

6.1 Models for J/ψ production

The models of inelastic and diffractive J/ψ productions are described together with elastic J/ψ production in this section, since the former forms background to the latter. Events are generated according to the differential cross section. The strategy of cross section calculation is depicted below.

While scattering actually consists of an infinite number of subprocesses, it can often be treated as a three-step process. In the first step, some soft and semihard subprocesses happen as the two beam particles approach each other. In the case of photon for example, it may fluctuate into a pair of $q\bar{q}$, or even hadronize into light vector mesons as conjectured in the vector-meson-dominance model, depending on the hard scale of the second step. In the second step, hard scattering between two particles or partons occurs within an extremely short space-time distance. This step is largely responsible for how an event looks like in the detector. Then after some soft and semi-hard subprocesses, hadrons are formed in the third step. Subprocesses in the third step, e.g. decay of J/ψ, have no influence on the production cross section. In a cross section calculation, scattering is accordingly *factorized* into flux factors corresponding to the first step, a hard subprocess corresponding to the second step, and the probability for a specified final hadronic state to occur in the third step.

6.1.1 Inelastic J/ψ production

At very small Q^2, ep scattering factorizes into an equivalent photon flux($e \to e\gamma$ as shown in Figure 32(a)) and a γp process. The reaction $e \to e\gamma$ as a calculable QED process is well described by the Equivalent Photon Approximation(EPA) as explained in Chapter II. The spectrum of the quasi-real photon flux is given by:

$$f_{\gamma/e}\left(y, Q^2\right) = \frac{\alpha}{\pi y Q^2}\left(1 - y + \frac{y^2}{2} - \frac{m_e^2 y}{Q^2}\right) \tag{51}$$

where y is the fraction of electron energy carried by the photon and Q^2 measures the virtuality of the photon. The ep cross section and γp cross section are related by

$$\frac{d\sigma_{ep}}{dy} = \sigma_{\gamma p}\left(y\right) f_{\gamma/e}\left(y\right) \quad . \tag{52}$$

where Q^2 is integrated out. Eq. (52) is an example of factorization. Following this strategy, $\sigma_{\gamma p}$ can be further factorized if a suitable harder scale exists. In the case of inelastic J/ψ photoproduction, the γp process is factorized into $p \to gX$ as shown in Figure 32(b) and γg processes, where X stands for the proton remnant. The spectrum of gluon flux associated with the proton is described by the gluon distribution function $G(x, \mu^2)$, where x is the fraction of proton momentum carried by the gluon, and $\mu^2(\sim m_{J/\psi}^2)$ is a hard scale for the $p \to gX$ process. Then

$$\sigma_{\gamma p} = \int dx d\hat{t} G\left(x, \mu^2\right) \frac{1}{16\pi\hat{s}^2}|M|^2 \tag{53}$$

where M is the amplitude of the γg fusion process, $\hat{s} = xys$ and $\hat{t} = (\gamma - \psi)^2$. $\hat{s}$ and $\hat{t}$ are two kinematic variables characterizing the hard subprocess. Calculation of $\gamma g \to c\bar{c}g \to J/\psi g$ will be discussed later.

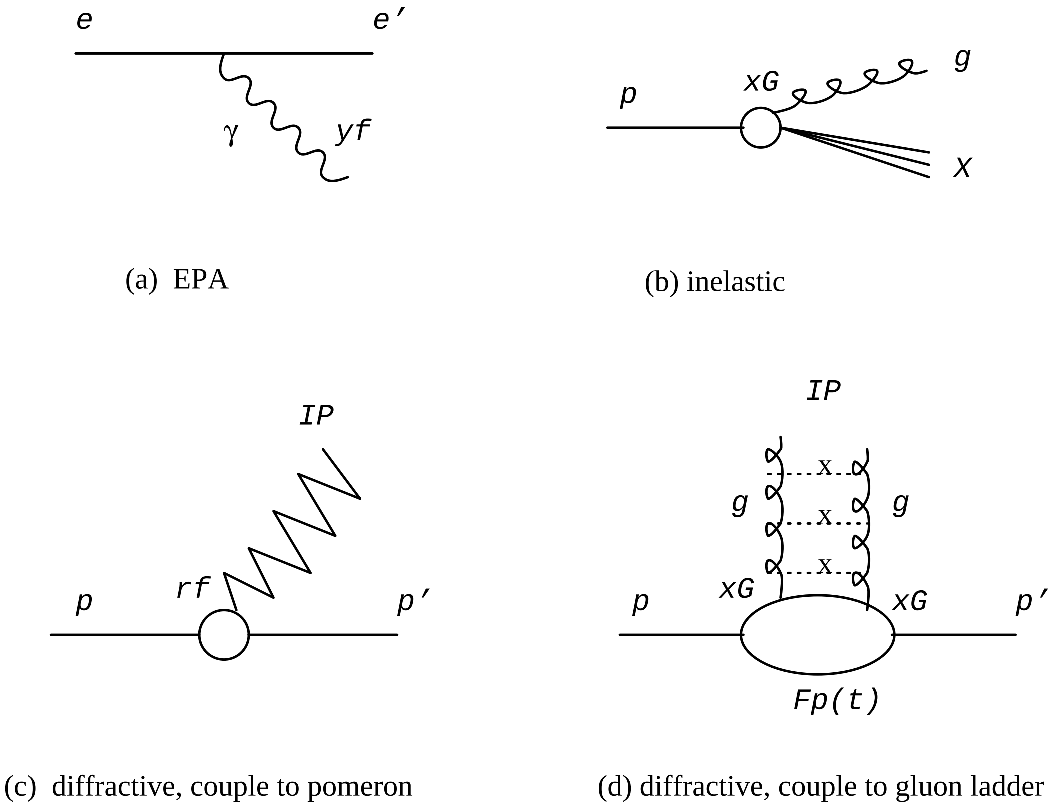

Figure 32: Models for soft processes used in J/ψ Monte Carlo generators. (a) $e \to e'\gamma$ is a QED process. The spectrum $yf_{\gamma/e}(y, Q^2)$ is described by the EPA formula. (b) Inelastic $p \to gX$ is described by proton structure function $xG(x, \mu^2)$. (c) Diffractive process with a pomeron emitted from a proton. The pomeron spectrum is empirically described by Eq. (54). (d) Diffractive process with the pomeron modeled as a gluon ladder.[60] Two gluons at the bottom couple to a proton by the proton structure function $\bar{x}G(\bar{x}, \bar{q}^2)$ and a two-gluon form factor $F_p^{2g}(t)$.

6.1.2 Elastic and diffractive J/ψ production

Similarly, in elastic scattering at small $|t|$, γp process is factorized into $p \to p I\!P$(see Figure 32(c)) and $\gamma I\!P$ processes. A notable difference between The pomeron flux generation $p \to p I\!P$ has been extensively studied in proton-proton collisions.[61,62] The pomeron spectrum $f_{I\!P/p}(t,r)$ is given as[63]

$$f_{I\!P/p}\left(t,r\right) = \frac{\beta^2_{pI\!P}\left(t\right)}{16\pi} r^{1-2\alpha_{I\!P}(t)} \tag{54}$$

where r is the momentum fraction $\frac{q\cdot I\!P}{q\cdot p}$, and

$$\begin{aligned}
\beta_{pI\!P}\left(t\right) &= \beta_{pI\!P}\left(0\right) e^{-\frac{1}{2}R_N^2|t|} \\
\alpha_{I\!P}\left(t\right) &= \alpha_{I\!P}\left(0\right) + \alpha' t + \hat{\epsilon} \\
R_N^2 &= 3.3\mathrm{GeV}^{-2}; \quad \beta_{pI\!P}\left(0\right) = 10\mathrm{GeV}^{-1}; \\
\alpha' &= 0.25\mathrm{GeV}^{-2}; \quad \hat{\epsilon} = 0.085
\end{aligned} \tag{55}$$

The function form is motivated by the pomeron model of diffractive scattering and the parameters are fixed by proton-proton(antiproton) diffractive scattering data. $\hat{\epsilon}$ is inserted[15] to account for the rising total cross section observed in $p\bar{p}$ and recently at HERA by ZEUS and H1 experiments.[29,h1photopaper] Then

$$\sigma_{\gamma p} = \int f_{I\!P/p}\left(t,r\right) \hat{\sigma}\left(\hat{s}\right) dr dt \tag{56}$$

If the pomeron is dissociated, then the $\gamma I\!P$ process is further factorized into $I\!P \to gX$ and γg processes. The γg process is the same as in inelastic J/ψ production case.

$$\sigma_{\gamma p} = \int f_{I\!P/p}\left(t,r\right) f_{g/I\!P}\left(x\right) \hat{\sigma}\left(\hat{s}\right) dr dx dt \tag{57}$$

where $f_{g/I\!P}(x)$ is the pomeron structure function. However, there is no guarantee that the proton vertex in $\gamma p \to J/\psi p$ can be treated the same way as in proton-proton diffractive scattering. This factorization is an assumption.

Another approach to diffractive scattering is to model the empirical pomeron as a gluon ladder which is a QCD object.[60] In this approach, γp process is factorized into $p \to p' gg$(as shown in Figure 32(d)) and $\gamma gg \to J/\psi$. The two gluons emitted from the proton must be in a color singlet configuration. The vertex of $pggp'$ is described by the square of $xG(x, \mu^2)$(i.e., two gluons are collinear) and a two-gluon form factor $F_p^{2g}(t)$ to account for t dependence of the cross section. The two gluons are bounded together by exchanging partons(schematically as rungs of the ladder) according to the LLA(Leading Logarithm Approximation). Next we explain calculations of the hard subprocesses.

6.1.3 The process $\gamma g \to c\bar{c}g \to J/\psi g$

First, we note that cross sections calculated by the lowest order QCD differ from experimental data in general. For example, the charm pair production via photon-gluon fusion(PGF) $\gamma g \to c\bar{c}$ is not completely calculable from perturbative QCD. The cross section for this process derived from the lowest order QCD calculation differs from the measured value by a factor of about 5 due to the effect of higher order QCD corrections. [64] Lowest order QCD calculations for the bound state J/ψ production via PGF suffer from the same problem.

The process $\gamma g \to J/\psi g$, as shown in Figure 33(a), has been calculated by two methods: the CS(Color Singlet) model[65] and the open charm method.[15,66] Both methods calculate the process $\gamma g \to c\bar{c}g$ using perturbative QCD, where a final state gluon is emitted from a $c(\bar{c})$ quark to satisfy color and spin constraints. However, the process $c\bar{c} \to J/\psi$ is treated differently in the two methods and therefore the constraints on the configuration of $c\bar{c}g$ are different. The spin constraint in the open charm method is not strict. In the CS model, the $c\bar{c}$ pair has the correct invariant mass($m_{J/\psi}$) and move more collinearly. The probability of $c\bar{c} \to J/\psi$ is determined by the wave function $|\psi(0)|^2$ which in turn can be determined from

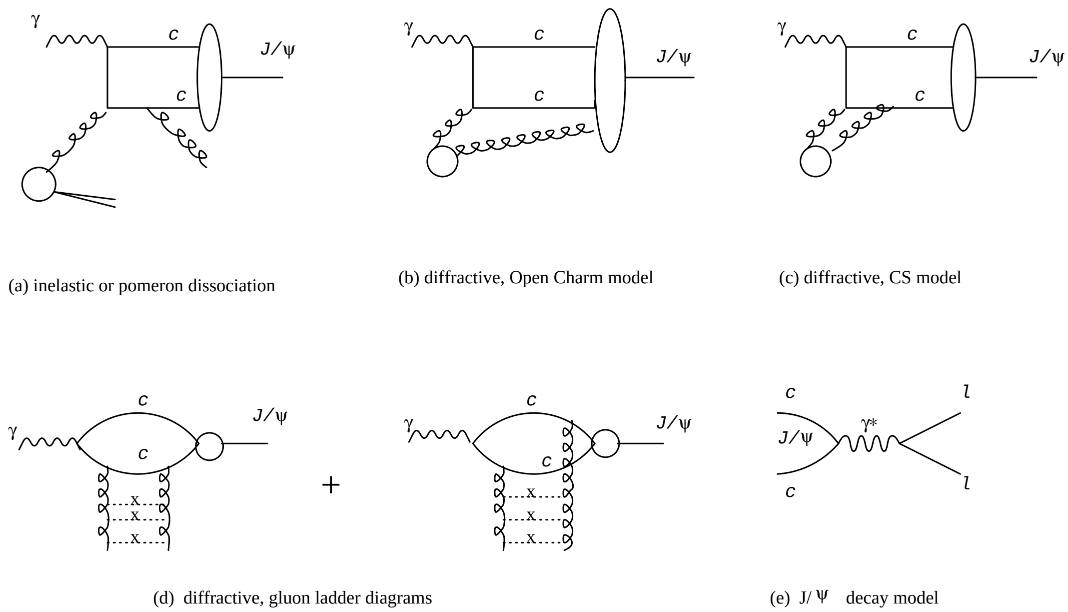

Figure 33: Feynman diagrams of the hard subprocesses in J/ψ production. (a) $\gamma g \rightarrow J/\psi g$ process. Only one Feynman diagram is shown as example. The gluon may be emitted from any charm quark line. In the case of inelastic J/ψ production, the gluon comes from the proton. In the case of diffractive dissociation of the pomeron, the gluon comes from the pomeron. The gluon spectrum is different in these two processes, but the amplitude of $\gamma g \rightarrow J/\psi g$ is the same. This process was calculated in the "open charm" model[65] and in the Color Singlet model.[66,15](b) and (c) The diffractive process using the pomeron model can also be calculated in two ways: The "open charm" method(b) and the Color Singlet model(c). In (c), only one Feynman diagram is shown as an example. (d) Diffractive process by gluon ladder. Two gluons may couple to either the same charm quark or different charm quarks. (e) QED model of J/ψ leptonic decay. The wave function at the center $|\psi(0)|$ can be derived from the measured leptonic decay width Γ_{ll} and be used to fix $c\bar{c} \rightarrow J/\psi$ in the CS model calculation.

the leptonic decay width of J/ψ using the Van Royen-Weisskopf formula:[67]

$$\Gamma\left(V \rightarrow l^{+}l^{-}\right) = \frac{16\pi\alpha^{2}|\sum_{i} a_{i}q_{i}|^{2}}{M_{V}^{2}}|\psi\left(0\right)|^{2} \tag{58}$$

In the case of J/ψ production, $|\sum_i a_i q_i|^2$ is simply q_c^2(charge of c quark squared). Eq. (58) is calculated from the QED process $c\bar{c} \to \gamma* \to l^+l^-$ (Figure 33(e)). With the QCD correction,[68] it becomes

$$\Gamma_{ll} = \Gamma_{ll}^{(0)} \left(1 - \frac{16}{3}\frac{\alpha_s}{\pi}\right) \tag{59}$$

where $\Gamma_{ll} = 5.36 \pm 0.29$KeV is the experimental value[70] which has changed noticeably in the last few years, and $\Gamma_{ll}^{(0)}$ is the uncorrected QED result which is used to determine $|\psi(0)|^2$. In the non-relativistic CS calculation,[65] the relative motion of $c\bar{c}$ inside J/ψ is neglected. Then $m_c = m_{J/\psi}/2$, and c and $\bar{c}$ move with the same momentum. The non-relativistic CS calculation describes data for $z < 0.9$ reasonably well but underestimates the cross section for $z > 0.9$.[15], where $z = p \cdot \psi / p \cdot q$ was defined in Eq. (6). Recently, it was shown that by taking into account internal motions of $c\bar{c}$(relativistic corrections), agreement between the CS model and the experimental data in the whole range of z is much improved.[72] One consequence of the internal motion is that $m_{J/\psi} = 2m_c + \epsilon$, i.e., $m_c \neq m_{J/\psi}/2$. Another consequence is that $c\bar{c}$ configuration is less constrained. Both consequences lead to a larger cross section especially at high z. $\epsilon/m_c \approx 0.16$($m_c = 1.43$GeV) is determined from J/ψ decay data.[69,70] A $K \approx 2$ factor is needed to include higher order QCD effects.

In the "open charm" approach, $\gamma g \to c\bar{c}g$ is calculated for a less constrained configuration of $c\bar{c}$. The constraints are $c\bar{c}$ be a color singlet and spin 1(approximately), and the invariant mass be below the threshold of production of two D mesons($m_D \approx 1.87$GeV). $c\bar{c} \to J/\psi$ is handled by the subroutines in the CERN LUND program[74] in the Monte Carlo generator. Since $\gamma g \to c\bar{c}g$ is not infrared finite(while it is finite in the CS model), a cut on transverse momentum of the final state gluon($p_\perp > 0.1$GeV) is made. A corresponding cut on $p_\perp$ of J/ψ should be made in the experimental data.

6.1.4 The process $\gamma I\!P \rightarrow J/\psi$

The diagram of the pomeron emission from the proton was shown previously in Figure 32(c). At the proton side, $|t| < 0.5\text{GeV}^2$ is too small to allow QCD calculations. At the $\gamma I\!P J/\psi$ vertex, the c quark mass(1.55GeV) provides a hard scale which allows partonic content of the pomeron be probed. A pomeron is then modeled as consisting of two gluons in the hard process(see Figure 33(b) and(c)). As in $\gamma g \rightarrow J/\psi g$, $\gamma I\!P \rightarrow J/\psi$ can also be calculated in two ways, using the "open charm" method and the CS model. In the open charm method, the $I\!P$ is modeled as two gluons described by the pomeron structure function(Figure 33(b)). $\gamma g \rightarrow c\bar{c}$ is calculated from QCD, where g is one gluon from the $I\!P$. Then $c\bar{c}g \rightarrow J/\psi$ is handled by the LUND program, where g is the other gluon(or the pomeron remnant) from the $I\!P$.

In the CS model(Figure 33(c)), $\gamma gg \rightarrow c\bar{c} \rightarrow J/\psi$ is calculated with relativistic corrections. Note that Figure 33(c) only shows one Feynman diagram as an example. Two gluons coupling to different charm quarks, for example, is also included in the matrix element calculation. The $I\!P$ is modeled as a color singlet and spin 1 bound state of two gluons with an assumed harmonic wave function which peaks at $x_g = 1/2$(each gluon carries one half of the pomeron momentum). The actual calculation is done for two collinear gluons. The $c\bar{c} \rightarrow J/\psi$ probability is determined from $\Gamma_{ll}^{(0)}$ as in the inelastic CS calculation. Note that the gluon distribution in the pomeron is modeled differently in the CS model and the open charm method.

6.1.5 The process $\gamma gg \to J/\psi$

In this approach, the $I\!P$ is modeled by a gluon ladder. Further more, the coupling of the gluon ladder with the proton is not described by the empirical function in Eq. (54), but from the proton structure function and form factor(see below). The two Feynman diagrams are shown in Figure 33(d). The bottom of the gluon ladder couples to the proton instead of the pomeron. The cross section is found to be

$$\frac{d\sigma_{\gamma p\to J/\psi p}}{dt} = \left[F_p^{2g}(t)\right]^2 \frac{\alpha_s^2 \Gamma_{ll} m_{J/\psi}^3 \pi^3}{3\alpha} \left[\bar{x}G\left(\bar{x},\bar{q}^2\right)\frac{2\bar{q}^2 - p_t^2}{\left(2\bar{q}^2\right)^3}\right]^2 \left(1+\frac{Q^2}{m_{J/\psi}^2}\right) \quad (60)$$

$$\bar{q}^2 = \frac{m_{J/\psi}^2 + Q^2 + p_t^2}{4}; \quad \bar{x} = \frac{m_{J/\psi}^2 + Q^2 + p_t^2}{s_{\gamma p}} \quad (61)$$

where $\bar{x} \approx q \cdot I\!P / q \cdot p$ is the fraction of the proton momentum carried by the pomeron, $\bar{q}^2$ is a hard scale, $G(\bar{x},\bar{q}^2)$ is the gluon distribution function associated with the proton, and F_p^{2g} is a two-gluon form factor which characterizes correlation between two gluons inside the proton. $F_p^{2g} = 1$ at $t = 0$. In Monte Carlo studies, the electromagnetic proton structure function $F_p^{em}(t) = (1 - \frac{t}{0.71\mathrm{GeV}^2})^{-2}$ is used as F_p^{2g}, although it is an unknown function and should be measured experimentally, strictly speaking.

6.2 Monte Carlo generators

Four MC event samples were used in this analysis. Three events samples EPJPSI 11, EPJPSI 12 and EPJPSI 13 were generated by EPJPSI(version 3.3)[71]. One event sample DIPSI was generated by DIPSI(version 1)[73].

EPJPSI can be used to generate J/ψ produced in a variety of beams and via various mechanisms. In our study, EPJPSI was used to generate events for the following processes: